Available online at www.sciencedirect.com
ScienceDirect
Journal of Sound and Vibration 299 (2007) 64–82
JOURNAL OF SOUND AND VIBRATION
www.elsevier.com/locate/jsvi

Nonlinear parametric instability of wind turbine wings

J.W. Larsen*, S.R.K. Nielsen

Department of Civil Engineering, Aalborg University, Sohngaardsholmsvej 57, DK-9000 Aalborg, Denmark

Received 8 March 2005; received in revised form 21 June 2006; accepted 27 June 2006
Available online 20 September 2006

Abstract

Nonlinear rotor dynamic is characterized by parametric excitation of both linear and nonlinear terms caused by centrifugal and Coriolis forces when formulated in a moving frame of reference. Assuming harmonically varying support point motions from the tower, the nonlinear parametric instability of a wind turbine wing has been analysed based on a two-degrees-of-freedom model with one modal coordinate representing the vibrations in the blade direction and the other vibrations in edgewise direction. The functional basis for the eigenmode expansion has been taken as the linear undamped fixed-base eigenmodes. It turns out that the system becomes unstable at certain excitation amplitudes and frequencies. If the ratio between the support point motion and the rotational frequency of the rotor is rational, the response becomes periodic, and Floquet theory may be used to determine instability. In reality the indicated frequency ratio may be irrational in which case the response is shown to be quasi-periodic, rendering the Floquet theory useless. Moreover, as the excitation frequency exceeds the eigenfrequency in the edgewise direction, the response may become chaotic. For this reason stability of the system has in all cases been evaluated based on a Lyapunov exponent approach. Stability boundaries are determined as a function of the amplitude and frequency of the support point motion, the rotational speed, damping ratios and eigenfrequencies in the blade and edgewise directions.

1. Introduction

Nonlinear rotor dynamic is characterized by parametric excitation when formulated in a moving frame of reference, in combination with the translational and rotational support point motions of the hub. Specific for wind turbine wings is that the parametric excitation is controlled by four different frequencies. First, the wing is rotating with the circular frequency Ω_0, the so-called rotational speed, which causes both parametric and additive excitations of the wing. The tower performs narrow-banded vibrations with a central circular frequency ω_0, which causes correspondingly support point motions and rotations of the hub. For a three-bladed wind turbine ω_0 is close to $3\Omega_0$ due to the changes in the wind load when the individual wings are in top and bottom positions of the incoming shear wind field. Finally, nonlinear interactions and related parametric instability depend on the ratio between the fundamental fixed base circular eigenfrequencies ω_1 and ω_2 in the blade and edgewise directions. For larger wind turbine wings the frequency ratio $\omega_2/\omega_1 \simeq 2$ is often met. The indicated almost rational frequency ratio may induce specific so-called 2:1 internal resonances and related

*Corresponding author. Tel.: +45 9635 7230; fax: +45 9814 2555.
E-mail address: i5jwl@civil.aau.dk (J.W. Larsen).

0022-460X/$ - see front matter © 2006 Elsevier Ltd. All rights reserved.
doi:10.1016/j.jsv.2006.06.055

parametric instabilities. Larsen and Nielsen [1] derived the nonlinear rotor equations of motion retaining up to cubic inertial and geometric nonlinear coupling terms for a rotating Bernoulli–Euler beam subjected to support point motion. The equations of motion were reduced to a two-degrees-of-freedom (2dof) system by a truncated modal expansion with one degree-of-freedom (1dof) in the blade direction and 1dof in the edgewise direction. The important nonlinear coupling terms under 2:1 internal resonance due to harmonically varying support point motion were identified, and the reduced system was analysed with respect to variable modal damping and excitation amplitude.

Stability of motions may be studied by a variety of techniques. A quantitative stability analysis of nonlinear systems may be performed by various perturbation methods, see e.g. Ref. [2]. For nonlinear systems, which experience periodic response, the stability may be analysed by the Floquet theory [3]. Nonlinear systems may experience almost periodic or even chaotic response. Under such conditions the Floquet theory is no longer applicable. To investigate the stability of such cases techniques based on a Lyapunov exponent may be used. Wolf et al. [4] presented an algorithm for determining the entire spectrum of Lyapunov exponents from a time series of displacement components by means of the Gram–Schmidt reorthonormalization procedure. Also algorithms for finding only the largest Lyapunov exponent or the two largest Lyapunov exponents were devised. The procedures described by Wolf et al. are widely used in the literature.

Several extensive investigations on the onset of chaotic motions of the Duffing oscillator have been performed based on these algorithms, see e.g. Refs. [5,6]. To and Liu [7] investigated the chaotic behaviour of the Duffing oscillator both under deterministic, stochastic and combined deterministic and stochastic excitations by means of an averaged Lyapunov exponent and information dimension. Castanier and Pierre [8] analysed wave propagation and localization phenomena in multi-coupled systems using both the algorithm by Wolf et al. and a perturbation technique for finding the first Lyapunov exponent. Comparison of the said methods and Monte Carlo analysis were made, and good agreement was demonstrated in several cases. Shin and Hammond [9] showed that the conventional Lyapunov exponent is very useful for quantification of chaotic dynamics, but only represent the average long-term behaviour. They introduced the so-called instantaneous Lyapunov exponents for describing the local non-stationary behaviour of the system. Numerical examples were given for the Van der Pol and Duffing oscillators, where changes in damping were detected efficiently. The theory was also used to determine changes in damping properties of an experimental system.

Parametric excitation due to support point motion of nonlinear systems is also widely investigated in the literature. Ge and Tsen [10] analysed the dynamic behaviour of a 2dof rigid body with vibrating support. The Lyapunov direct method was used to determine the stability conditions, and various algorithms were used to effectively control the chaotic behaviour. In the same manner Ge and Shiue [11] analysed the dynamic stability of a tachometer subjected to vertical harmonic support vibrations. In a series of papers Dwivedy and Kar [12–16] investigated the parametric stability of a base excited cantilever beam with an attached mass retaining up to cubic nonlinearities. They analysed the steady state, periodic and chaotic responses under parametric and internal resonances by the methods of multiple scales and normal forms. Nayfeh [17] analysed a 2dof nonlinear system with quadratic nonlinearities subjected to parametric excitation, and a multi-degrees-of-freedom system under parametric excitation in Ref. [18]. Hanagud and Sarkar [19] analysed a cantilever beam attached to a moving support. The formulation was shown to be valid for large displacements, and the stability characteristics of a beam under spin-up manoeuvre was studied. It was demonstrated that structural nonlinearities play a major role in the response characteristics.

The present paper deals with the onset of chaotic behaviour and parametric instability of nonlinear vibrations of wind turbine wings. In this study, which is based on the reduced 2dof model by Larsen and Nielsen [1], the amplitude, the frequency of the support point motion and the rotational speed are varied, along with the eigenfrequency ratio ω_2/ω_1 and the damping ratio ζ_1 of the blade mode. The damping ratio may vary significantly dependent on the characteristics of the boundary layer flow over the profile. The flow may be fully attached, partly separated or fully separated. The latter case occurs during large oscillations (dynamic stall), with the implication that the significant aerodynamic damping during fully attached flow conditions is lost. When the ratio between the tower frequency and rotational frequency ω_0/Ω_0 is rational the response becomes periodic and stability of the solution at certain parameter values may be evaluated using Floquet theory. If the response becomes chaotic or almost periodic due to irrational excitation frequency

ratios and nonlinear effects the Floquet theory is no longer applicable. Instead the stability may be evaluated using the Lyapunov coefficient. Since, the Floquet theory only is applicable in small regions of the investigated parameter space, the Lyapunov exponent approach will be used to determine stability of the system throughout this study. Due to the often met frequency ratios of $\omega_2/\omega_1 \simeq 2$ and $\omega_0/\Omega_0 \simeq 3$ the following analyses are focused around these.

2. Modelling of the system

2.1. Geometrical description

A global (x_1, x_2, x_3)-coordinate system is placed at the bottom of the tower with the x_1-axis oriented parallel to the rotor axes as shown in Fig. 1. To simplify matters the tilt angle and the cone angle of the wind turbine are assumed to be zero. The tower–nacelle system deforms a rotation and displacement of the hub occurs, which introduce a rotation of the rotor plane. Additionally, a blade fixed (x'_1, x'_2, x'_3)-coordinate system with origin at the hub and with the (x'_2, x'_3)-plane is introduced parallel to the global (x_2, x_3)-plane when the tower is not deflected. The position of the x'_2-axis is determined by the phase angle $\Phi(t)$ from the global x_2-axis to the local x'_2-axis with the sign definition shown in Fig. 1b. The x'_3-axis is oriented from the hub towards the free end. Then, the x'_1- and x'_2-axes define the blade and edgewise directions, respectively. The shear centres of the cross sections along the beam are assumed to be positioned on the x'_3-axis.

The wing is decoupled from the nacelle and the tower by introducing prescribed linear translation and rotation vectors $\mathbf{u}_0(t)$ and $\boldsymbol{\theta}_0(t)$ with the global and local coordinates $u_{i,0}(t)$, $\theta_{i,0}(t)$ and $u'_{i,0}(t)$, $\theta'_{i,0}(t)$. To simplify matters further, only the deformation components $u_{1,0}(t)$ and $\theta_{2,0}(t)$ are considered, as shown in Fig. 1b. Additionally, these components, which are causing quasi-static displacements merely in the blade direction, are assumed to be related through the fundamental eigenmode of the tower. Hence, the following support point motions are assumed:

$$u_{1,0}(t) = u(t), \quad \theta_{2,0}(t) = \Theta_{2,0}u(t), \quad u_{2,0}(t) = u_{3,0}(t) = \theta_{1,0}(t) = \theta_{3,0}(t) = 0. \tag{1}$$

The modal coordinate of the tower $u(t)$ may be interpreted as the physical horizontal displacement of the nacelle.

The base unit vectors of the fixed (x_1, x_2, x_3) and the movable (x'_1, x'_2, x'_3)-coordinate system are denoted as $\mathbf{i}_j$ and $\mathbf{i}'_j(t)$, $j = 1, 2, 3$, respectively. The transformation between the said base vectors and the local and global components v'_i and v_j of a vector $\mathbf{v}$ is given as

$$\mathbf{i}'_i(t) = A_{ij}(t)\mathbf{i}_j, \quad v'_i = A_{ij}(t)v_j. \tag{2}$$

In Eq. (2) and below the summation convention over dummy indices has been applied. Dummy Latin indices range over 1, 2 and 3, and dummy Greek indices over 1 and 2.

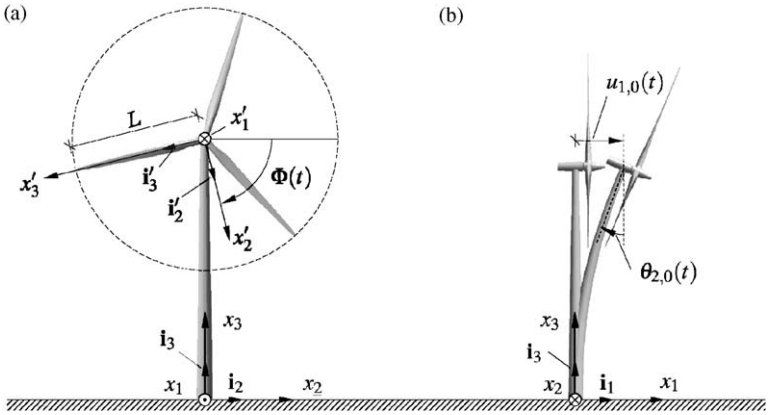

Fig. 1. Definitions of coordinate systems and support point deformation.

The coordinate transformation matrix $\mathbf{A}(t)$ is found to be

$$\mathbf{A}(t) = \begin{bmatrix} -1 & 0 & 0 \\ 0 & \cos\Phi & -\sin\Phi \\ 0 & -\sin\Phi & -\cos\Phi \end{bmatrix} \begin{bmatrix} \cos\theta_{2,0} & 0 & -\sin\theta_{2,0} \\ 0 & 1 & 0 \\ \sin\theta_{2,0} & 0 & \cos\theta_{2,0} \end{bmatrix}. \tag{3}$$

The time-derivative of $\Phi(t)$ specifies the rotational frequency of the rotor

$$\Omega(t) = \dot{\Phi}(t). \tag{4}$$

Then the local components of the support point motion become $u'_{i,0}(t) = A_{i1}(t)u(t)$ and $\theta'_{i,0}(t) = A_{i2}\Theta_{2,0}u(t)$. Hence, the local components become

$$\mathbf{u}'_0(t) = \begin{bmatrix} -u(t)\cos\theta_{2,0} \\ -u(t)\sin\Phi\sin\theta_{2,0} \\ -u(t)\cos\Phi\sin\theta_{2,0} \end{bmatrix}, \quad \boldsymbol{\theta}'_0(t) = \begin{bmatrix} 0 \\ \Theta_{2,0}u(t)\cos\Phi \\ -\Theta_{2,0}u(t)\sin\Phi \end{bmatrix}. \tag{5}$$

To simplify matters, the effects on the hub displacement from the rotation $\theta_{2,0}$ are disregarded. Hence, $u'_{1,0}(t) \simeq -u(t)$, $u'_{2,0}(t) = u'_{3,0}(t) \simeq 0$.

2.2. Modal equations of motion

In order to discretize the variational equations, obtained from the principle of virtual work in Larsen and Nielsen [1], the displacement components $u'_\alpha(x'_3, t)$ and the variational field $\delta u'_\alpha(x'_3)$ are represented by the following modal expansion:

$$u'_\alpha(x'_3, t) \simeq \sum_{j=1}^{\infty} \Phi_\alpha^{(j)}(x'_3)q_j(t), \quad \delta u'_\alpha(x'_3, t) = \sum_{j=1}^{\infty} \Phi_\alpha^{(j)}(x'_3)\delta q_j(t), \tag{6}$$

where $u'_1(x'_3, t)$ is the deformation component in the blade direction and $u'_2(x'_3, t)$ is the deformation component in the edgewise direction. $q_j(t)$ denotes the modal coordinates and $\Phi_\alpha^{(j)}(x'_3)$ represents the undamped eigenmodes, where upper index denotes the mode number and lower index indicates the component. $\Phi_\alpha^{(j)}(x'_3)$ has been solved by means of an finite element method, which also provides all necessary derivatives of the eigenmodes. The eigenmodes have been determined for a constant referential rotational frequency Ω_0 in such a way that they decouple the constant linear terms together with a quasi-static referential contribution due to centrifugal force from Ω_0. The self-adjoint eigenvalue problem for determining $\Phi_\alpha^{(j)}(x'_3)$ is given in Larsen and Nielsen [1].

Eq. (6) is used in the variational equation. Assuming that the rotational speed is constant, i.e. $\Omega(t) = \Omega_0$, then the mode shapes decouple the non-gyroscopic linear terms in the variational equations. The resulting ordinary differential equations for the modal coordinates when including all terms become

$$\begin{aligned} &\sum_{j=1}^{\infty}(m_{ij}\ddot{q}_j + c_{ij}(t)\dot{q}_j + k_{ij}(t)q_j) + \sum_{j=1}^{\infty}\sum_{k=1}^{\infty}(a_{ijk}(t)q_jq_k + b_{ijk}(t)q_j\dot{q}_k) \\ &\quad + \sum_{j=1}^{\infty}\sum_{k=1}^{\infty}\sum_{l=1}^{\infty}(d_{ijkl}q_jq_kq_l + g_{ijkl}(q_j\dot{q}_k\dot{q}_l + q_jq_k\ddot{q}_l)) = f_i(t), \end{aligned} \tag{7}$$

where

$$\begin{aligned} m_{ij} &= M_i\delta_{ij}, \\ c_{ij}(t) &= 2\zeta_i\omega_iM_i\delta_{ij} + \int_0^L \mu\Phi_\alpha^{(i)}E_{\alpha\beta}\Phi_\beta^{(j)}\,\mathrm{d}x'_3, \\ k_{ij}(t) &= M_i\omega_i^2\delta_{ij} + \int_0^L \left[\mu\Phi_\alpha^{(i)}D_{\alpha\beta}\Phi_\beta^{(j)} - \frac{\partial\Phi_\alpha^{(i)}}{\partial x'_3}\frac{\partial\Phi_\alpha^{(j)}}{\partial x'_3}\int_{x'_3}^L \mu D_{33}x'_3\,\mathrm{d}x'_3\right]\mathrm{d}x'_3. \end{aligned} \tag{8}$$

In Eq. (8) and below the summation convention has been abandoned over the modal coordinate indices. The components of **D** and **E** specify centrifugal and various Coriolis acceleration terms, respectively, and are given as

$$\mathbf{E}(t) = 2\begin{bmatrix} 0 & -\dot{\theta}'_{3,0} & \dot{\theta}'_{2,0} \\ \dot{\theta}'_{3,0} & 0 & -\Omega \\ -\dot{\theta}'_{2,0} & \Omega & 0 \end{bmatrix},$$

$$\mathbf{D}(t) = \begin{bmatrix} \dot{\theta}'^2_{3,0} + \dot{\theta}'^2_{2,0} & -\dot{\theta}'_{2,0}\Omega + \ddot{\theta}'_{3,0} & -\dot{\theta}'_{3,0}\Omega - \ddot{\theta}'_{2,0} \\ -\dot{\theta}'_{2,0}\Omega - \ddot{\theta}'_{3,0} & \dot{\theta}'^2_{3,0} + \Omega^2 & -\dot{\theta}'_{3,0}\dot{\theta}'_{2,0} + \dot{\Omega} \\ -\dot{\theta}'_{3,0}\Omega + \ddot{\theta}'_{2,0} & -\dot{\theta}'_{3,0}\dot{\theta}'_{2,0} - \dot{\Omega} & \dot{\theta}'^2_{2,0} + \Omega^2 \end{bmatrix}. \tag{9}$$

Further, in $c_{ij}(t)$ a damping term has been introduced via the modal damping ratio ζ_i accounting for structural and aerodynamic damping. As seen, the first and second derivatives of the support point rotations $\theta'_{2,0}(t)$ and $\theta'_{3,0}(t)$ cause parametric excitation in the linear terms. The nonlinear coupling coefficients in Eq. (7) are defined as follows:

$$\begin{aligned}
a_{ijk}(t) &= \int_0^L \left[\frac{\partial \Phi_\alpha^{(i)}}{\partial x'_3} \frac{\partial \Phi_\alpha^{(j)}}{\partial x'_3} \int_{x'_3}^L \left[-p''_{\beta,A} \frac{\partial \Phi_\beta^{(k)}}{\partial x'_3} - \mu D_{3\beta} \Phi_\beta^{(k)} \right] \mathrm{d}x'_3 + \frac{1}{2} \Phi_\alpha^{(i)} p''_{\beta,A} \frac{\partial \Phi_\alpha^{(j)}}{\partial x'_3} \frac{\partial \Phi_\beta^{(k)}}{\partial x'_3} \right] \mathrm{d}x'_3, \\
b_{ijk}(t) &= \int_0^L \left[\frac{\partial \Phi_\alpha^{(i)}}{\partial x'_3} \frac{\partial \Phi_\alpha^{(j)}}{\partial x'_3} \int_{x'_3}^L -\mu E_{3\beta} \Phi_\beta^{(k)} \, \mathrm{d}x'_3 \right] \mathrm{d}x'_3, \\
d_{ijkl} &= \int_0^L \frac{1}{2} e_{\alpha\eta} E I''_{\alpha\beta} e_{\beta\xi} \left[\frac{\partial^2 \Phi_\eta^{(i)}}{\partial x'^2_3} \frac{\partial \Phi_\xi^{(j)}}{\partial x'_3} \frac{\partial \Phi_\gamma^{(k)}}{\partial x'_3} \frac{\partial^2 \Phi_\gamma^{(l)}}{\partial x'^2_3} + \frac{\partial^2 \Phi_\xi^{(l)}}{\partial x'^2_3} \frac{\partial \Phi_\eta^{(i)}}{\partial x'_3} \frac{\partial \Phi_\gamma^{(j)}}{\partial x'_3} \frac{\partial^2 \Phi_\gamma^{(k)}}{\partial x'^2_3} \right. \\
&\quad \left. + \frac{\partial^2 \Phi_\xi^{(l)}}{\partial x'^2_3} \frac{\partial \Phi_\eta^{(j)}}{\partial x'_3} \frac{\partial \Phi_\gamma^{(i)}}{\partial x'_3} \frac{\partial^2 \Phi_\gamma^{(k)}}{\partial x'^2_3} + \frac{\partial^2 \Phi_\xi^{(l)}}{\partial x'^2_3} \frac{\partial \Phi_\eta^{(j)}}{\partial x'_3} \frac{\partial \Phi_\gamma^{(k)}}{\partial x'_3} \frac{\partial^2 \Phi_\gamma^{(i)}}{\partial x'^2_3} \right] \mathrm{d}x'_3, \\
g_{ijkl} &= \int_0^L \left[\frac{\partial \Phi_\alpha^{(i)}}{\partial x'_3} \frac{\partial \Phi_\alpha^{(j)}}{\partial x'_3} \int_{x'_3}^L \left[\mu \int_0^{x'_3} \frac{\partial \Phi_\beta^{(k)}}{\partial x'_3} \frac{\partial \Phi_\beta^{(l)}}{\partial x'_3} \mathrm{d}x'_3 \right] \mathrm{d}x'_3 \right] \mathrm{d}x'_3, \\
f_i(t) &= \int_0^L \Phi_\alpha^{(i)} (p''_{\alpha,A} - \mu(\ddot{u}'_{\alpha,0} + D_{\alpha 3} x'_3)) \, \mathrm{d}x'_3.
\end{aligned} \tag{10}$$

As seen, the parametric excitation from $\theta'_{2,0}(t)$ and $\theta'_{3,0}(t)$ is also present in the quadratic nonlinear coupling terms $a_{ijk}(t)$ and $b_{ijk}(t)$. By contrast, the support point displacement $u'_{1,0}(t)$ only enters the equations as an additive load term via the modal loads $f_i(t)$. $b_{ijk}(t)$ and g_{ijkl} are quadratic and cubic nonlinear coupling coefficients originating from inertial nonlinearities, whereas d_{ijkl} is a purely geometrical nonlinear term from the nonlinear description of the curvature. The quadratic nonlinear coupling coefficients $a_{ijk}(t)$ include both contributions from the rotation of the aeroelastic loads and from the support point rotations. The parameters E and $I''_{\alpha\beta}$ are the elasticity module and the moment of inertia, respectively. $p''_{\alpha,A}$ indicates the aerodynamic loading, which is approximated by a harmonic variation with the rotational frequency Ω_0. The same variation was also assumed in Larsen and Nielsen [1]. As a result of the rotation during deformation of the beam, the fixed basis $(\mathbf{i}'_1, \mathbf{i}'_2, \mathbf{i}'_3)$ is rotated into a new basis $(\mathbf{i}''_1, \mathbf{i}''_2, \mathbf{i}''_3)$ defining a local (x''_1, x''_2, x''_3) coordinate system. $I''_{\alpha\beta}$ and $p''_{\alpha,A}$ are determined in this deformed coordinate system.

In the following numerical analyses only the two lowest modes are retained in the modal expansion. The components of the modal modes are given in Appendix A together with the wing characteristics including chord length, thickness, moment of inertia and mass distribution throughout the wing. Larsen and Nielsen [1] found that the equations of motion of the modal coordinates may be reduced without significant changes in

the frequency response. The reduced equations are used in the following analyses and are given as

$$\begin{aligned}
&M_1(\ddot{q}_1 + 2\zeta_1\omega_1\dot{q}_1 + \omega_1^2 q_1) + c_{12}(t)\dot{q}_2 + k_{11}(t)q_1 + k_{12}(t)q_2 + a_{111}(t)q_1^2 + (a_{112}(t) + a_{121}(t))q_1q_2 \\
&\quad + b_{111}(t)q_1\dot{q}_1 + b_{112}(t)q_1\dot{q}_2 + b_{121}(t)q_2\dot{q}_1 + d_{1111}q_1^3 + (d_{1112} + d_{1121} + d_{1211})q_1^2q_2 \\
&\quad + g_{1111}(q_1\dot{q}_1^2 + q_1^2\ddot{q}_1) + g_{1211}(q_2\dot{q}_1^2 + q_1q_2\ddot{q}_1) = f_1(t), \\
&M_2(\ddot{q}_2 + 2\zeta_2\omega_2\dot{q}_2 + \omega_2^2 q_2) + c_{21}(t)\dot{q}_1 + k_{21}(t)q_1 + k_{22}(t)q_2 + a_{211}(t)q_1^2 + (a_{212}(t) + a_{221}(t))q_1q_2 \\
&\quad + b_{211}(t)q_1\dot{q}_1 + b_{212}(t)q_1\dot{q}_2 + b_{221}(t)q_2\dot{q}_1 + d_{2111}q_1^3 + (d_{2112} + d_{2121} + d_{2211})q_1^2q_2 \\
&\quad + g_{2111}(q_1\dot{q}_1^2 + q_1^2\ddot{q}_1) + g_{2211}(q_2\dot{q}_1^2 + q_1q_2\ddot{q}_1) = f_2(t).
\end{aligned} \tag{11}$$

3. Harmonic response analysis

In the following the support point motion is assumed to vary harmonically with amplitude u_0 and circular frequency ω_0 as

$$u(t) = u_0 \cos\omega_0 t. \tag{12}$$

Hence, the excitation period is $T_0 = 2\pi/\omega_0$. The equations of motion (11) are solved numerically by means of a fourth-order Runge–Kutta method with a time step length of $\Delta t = T_0/500$ s and initial conditions $q_1(0) = q_2(0) = 1.0$ m, $\dot{q}_1(0) = \dot{q}_2(0) = 0.0$ m/s. Assuming harmonic support point motion together with harmonic variation of the aerodynamic loading the time-varying coefficients given in Eqs. (8) and (10) can be recast into time invariant coefficients multiplied by harmonic components. The coefficients are given in Appendix B. In the following Q_1 and Q_2 signify the rms value of $q_1(t)$ and $q_2(t)$ when averaged over one vibration period T. Initially, the eigenfrequency ratio $\omega_2/\omega_1 = 2$ is assumed, and the excitation frequency is specified as $\omega_0/\Omega_0 = 3$. Then, as seen from Eq. (B.1) the modal loads $f_1(t)$ and $f_2(t)$ contain harmonic components with the circular frequencies $m\Omega_0, m = 1,\ldots,4$. At first, the equations in Eq. (11) are considered when only the constant linear terms on the left-hand sides are retained, ignoring all linear parametric, quadratic parametric and cubic terms. The corresponding solution may be considered a zeroth-order solution in a perturbation approach, where the linear parametric terms, quadratic parametric terms and cubic terms represent various first-order perturbations, which are independently investigated below. The circular frequencies $m\Omega_0 = m/3\omega_0, m = 1,\ldots,4$, in the additive excitation terms will also be present in the zeroth-order solution. When any of these frequencies are equal to ω_1 or $\omega_2 = 2\omega_1$ resonance appears in the first and second modes. This happens for the excitation frequency ratios $\omega_0/\omega_1 = 3/m$ and $\omega_0/\omega_1 = 6/m$, respectively, as shown by the dashed curve on the frequency response curve in Fig. 2a.

The linear parametric coefficients $c_{ij}(t)$ and $k_{ij}(t)$ contain harmonic components with the circular frequencies $2\Omega_0$ and $4\Omega_0$. In combination with the harmonic components of the zeroth-order solution the linear parametric terms will contain harmonics at the circular frequencies $m\Omega_0 = m/3\Omega_0,\ m = 1,\ldots,8$. When transferred to the right-hand side these terms may induce resonance at $\omega_0/\omega_1 = 3/m$ and $\omega_0/\omega_1 = 6/m$, $m = 1,\ldots,8$ in the blade and edgewise modes, respectively. Hence, the resonance peaks for $m = 2,3,4$, present in the linear response, are influenced by the linear parametric excitation as well. However, as seen by the unbroken curve on Fig. 2a the influence of the linear parametric terms is insignificant in the blade mode, whereas the effect in the edgewise mode merely is to reduce the resonance frequencies and introduces weak coupling between the considered modes.

The quadratic parametric coefficients $a_{ijk}(t)$ and $b_{ijk}(t)$ contain harmonic components with the frequencies $1\Omega_0$, $2\Omega_0$ and $4\Omega_0$. In combination with the harmonic components of the zeroth-order solution the quadratic nonlinear terms will contain harmonics at the frequencies $m\Omega_0 = m/3\omega_0$, $m = 1,\ldots,12$. When transferred to the right-hand side these terms may induce resonance at $\omega_0/\omega_1 = 3/m$ and $\omega_0/\omega_1 = 6/m$, $m = 1,\ldots,12$. In Fig. 2b it is seen that the resonance peaks for $m = 2,3,4$ become unstable in the blade mode when quadratic nonlinear terms are included, which mean that these terms introduce parametric instability. In the edgewise mode resonance peaks are visible for $\omega_0/\omega_1 = 3/4$ and $\omega_0/\omega_1 = 1$ corresponding to $m = 4,6$. Additionally,

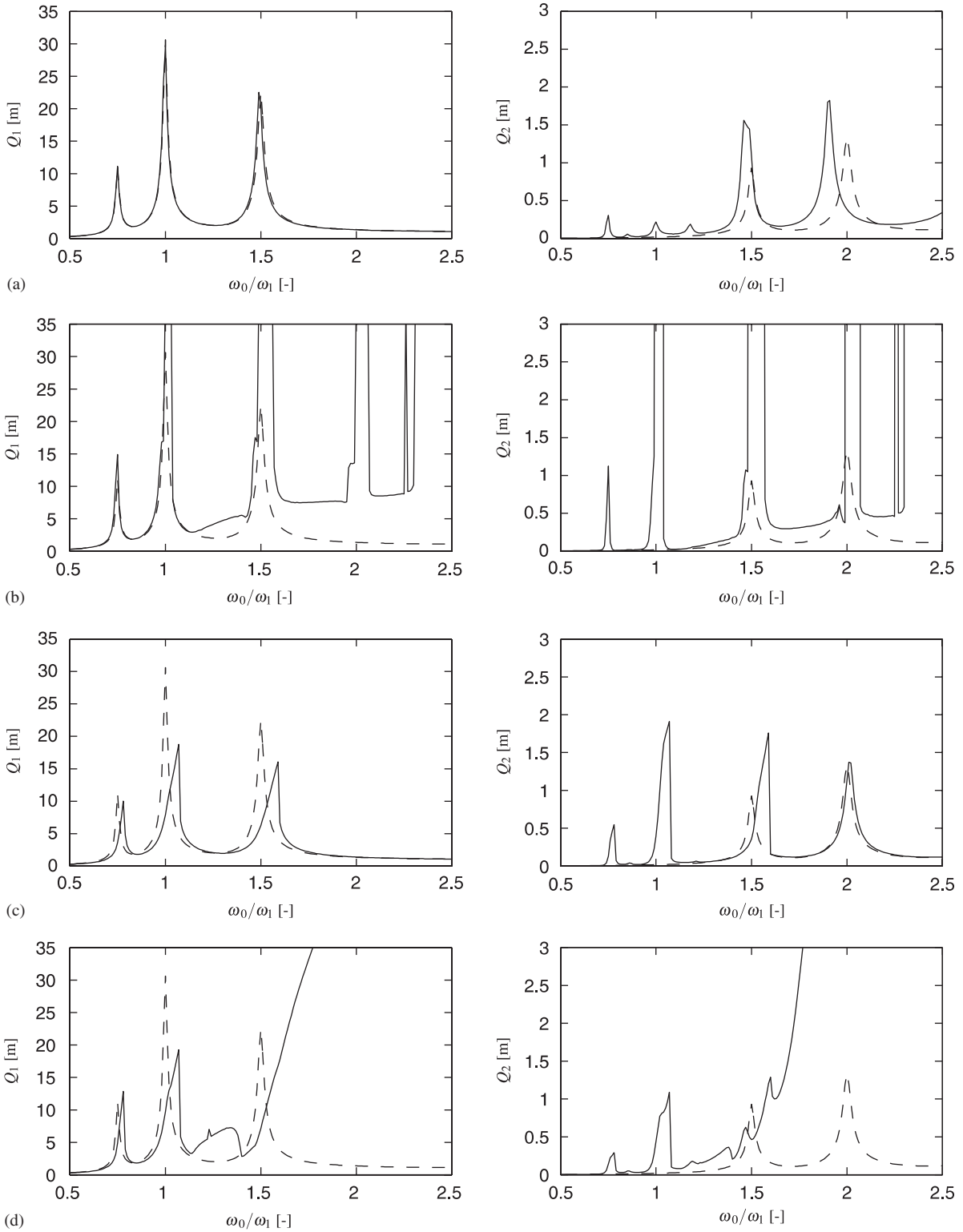

Fig. 2. Influence of linear parametric, quadratic parametric and cubic terms, $u_0 = 0.3\,\mathrm{m}$, $\zeta_1 = \zeta_2 = 0.01$, $\omega_0/\Omega_0 = 3.0$, $\omega_2/\omega_1 = 2.0$. (– –) Zeroth-order solution. (a) (—) Zeroth-order solution in combination with the linear parametric terms. (b) (—) Zeroth-order solution in combination with the quadratic parametric terms. (c) (—) Zeroth-order solution in combination with the cubic parametric terms. (d) (—) The full model.

chaotic behaviour or infinite response of the system may occur for $\omega_0/\omega_1 > 2$, corresponding to $\omega_0 > \omega_2$, which is not brought forward by the linear parametric terms.

The cubic zeroth-order solution terms contain harmonics at the frequencies $m\Omega_0 = m/3\omega_0$, $m = 1, \ldots, 12$. When transferred to the right-hand side these terms may induce resonance at $\omega_0/\omega_1 = 3/m$ and $\omega_0/\omega_1 = 6/m$, $m = 1, \ldots, 12$, as was the case for the quadratic parametric terms. In Fig. 2c it is seen that the cubic terms influence the blade mode by curving the resonance peaks to the right. In the edgewise mode extra resonance peaks occur for $\omega_0/\omega_1 \simeq 3/4$ and $\omega_0/\omega_1 \simeq 1.0$ corresponding to $m = 4, 6$, as was the case for the quadratic parametric terms.

Finally, in Fig. 2d the full model is compared with the linear response. Due to both the quadratic parametric terms and the cubic terms the response becomes chaotic for $\omega_0/\omega_1 > 1.5$. Comparison of Figs. 2b–d indicates that the response in the region $\omega_0/\omega_1 > 1.5$ is mainly influenced by the quadratic parametric terms, while at $\omega_0/\omega_1 < 1.5$ the cubic terms are the main source for changes compared to the zeroth-order solution.

It should be noted that at certain resonance peaks the deformation exceeds 30 m, which obviously is considered a failure situation. But considering the stability of the system a limited response is obtained when including the cubic terms. As mentioned, the cubic terms tend to curve the peaks, which give the possibility of multiple solutions at given frequencies, e.g. $\omega_0/\omega_1 \simeq 0.78$ and $\omega_0/\omega_1 \simeq 1.08$. However, the curving of the peaks is relatively small and multiple solutions are only obtained in a very narrow frequency band around the resonance peaks. The frequency response curves have been obtained from several different initial conditions. Identical curves are produced independent of the choice of initial conditions, and the possibility of multiple solutions has not been further investigated.

The additive loading includes among others the product of the harmonic components $\cos(\omega_0 t)$ and $\cos(\Omega_0 t)$, see Eq. (B.1). It turns out that the response period is determined from the interference of the response caused by the circular frequencies $\omega_0 + \Omega_0$ and $\omega_0 - \Omega_0$. The corresponding periods become

$$T^+ = \frac{2\pi}{\omega_0 + \Omega_0} = \frac{T_0}{1 + \Omega_0/\omega_0}, \quad T^- = \frac{2\pi}{\omega_0 - \Omega_0} = \frac{T_0}{1 - \Omega_0/\omega_0}. \tag{13}$$

In order to find the combined period of the response T the following ratios are evaluated

$$\frac{T}{T^+} = n\left(1 + \frac{m\Omega_0}{\omega_0}\right), \quad \frac{T}{T^-} = n\left(1 - \frac{m\Omega_0}{\omega_0}\right). \tag{14}$$

The factor n is found as the minimum value at which both T/T^+ and T/T^- attain integer values. Poincaré maps of 2000 excitation periods are plotted in Fig. 3 for various ratios of ω_0/Ω_0. The amplitude is $u_0 = 0.3$ m, the damping ratios $\zeta_1 = \zeta_2 = 0.01$ and the frequency ratio $\omega_0/\omega_1 = 0.8$. ($\circ$) indicate the phase value $(q_1, \dot{q}_1)$ for every excitation period T_0, and ($\times$) indicates the phase value at every response period T. As seen the period tends towards infinity as ω_0/Ω_0 becomes irrational. As an example $\omega_0/\Omega_0 = 3.14159$ results in $n = 314\,159$. For an irrational frequency ratio a so-called almost periodic response is achieved in which case a continuous closed curve is obtained in the phase plane for the Poincaré map. As seen from Fig. 3 the amplitude of $q_1(t)$ increases as ω_0/Ω_0 is increased. The reason is that the fundamental blade circular eigenfrequency for the considered example is given as $\omega_1/\Omega_0 = 3.2125$. Hence, the simulations tend towards resonance in the fundamental eigenmode as ω_0/Ω_0 is increased.

4. Parametric stability analysis

In order to investigate the stability of a given motion $q_{i,0}(t)$, consider the following perturbed motion assumed to fulfil (11)

$$q_i(t) = q_{i,0}(t) + \Delta q_i(t), \tag{15}$$

where $\Delta q_i(t)$ is a small perturbation to the referential solution. Insertion of Eq. (15) in Eq. (11) and disregarding quadratic and cubic terms of $\Delta q_i(t)$ gives the following equations of motion for the

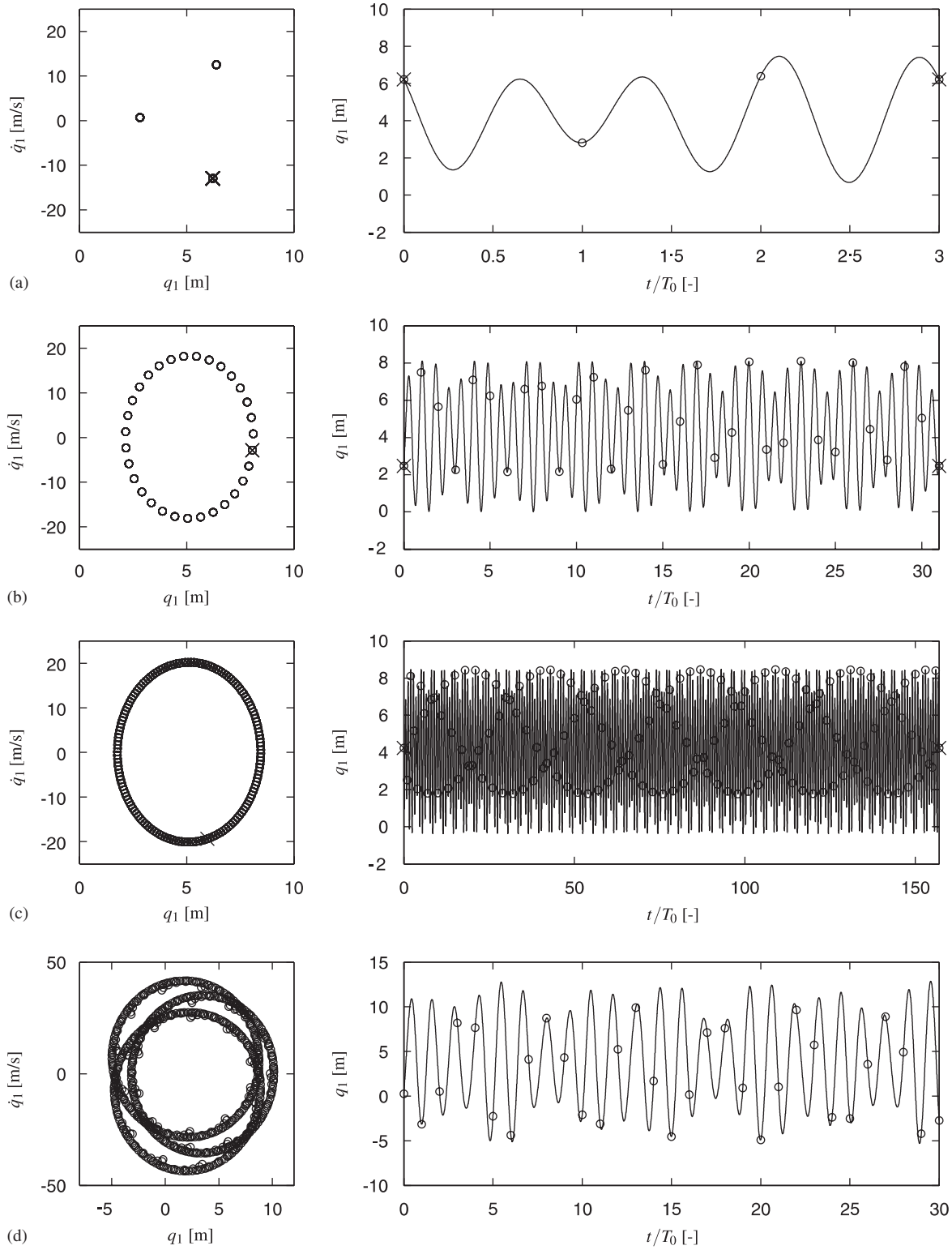

Fig. 3. Poincaré map at various excitations frequency ratios and the corresponding time series of $q_1(t)$ shown for one response period T. $u_0 = 0.3\,\mathrm{m}$, $\zeta_1 = \zeta_2 = 0.01$, $\omega_2/\omega_1 = 2.0$, $\omega_0/\omega_1 = 0.8$. (a) $\omega_0/\Omega_0 = 3$, $n = 3$. (b) $\omega_0/\Omega_0 = 3.1$, $n = 31$. (c) $\omega_0/\Omega_0 = 3.14$, $n = 157$. (d) Chaotic response, $\omega_0/\Omega_0 = 3$, $\omega_0/\omega_1 = 2.3$.

perturbation $\Delta q_i(t)$

$$
\begin{aligned}
&M_1(\Delta\ddot{q}_1 + 2\zeta_1\omega_1\Delta\dot{q}_1 + \omega_1^2\Delta q_1) + c_{12}(t)\Delta\dot{q}_2 + k_{11}(t)\Delta q_1 + k_{12}(t)\Delta q_2\\
&\quad + 2a_{111}(t)q_{1,0}\Delta q_1 + (a_{112}(t) + a_{121}(t))(q_{1,0}\Delta q_2 + q_{2,0}\Delta q_1)\\
&\quad + b_{111}(t)(q_{1,0}\Delta\dot{q}_1 + \dot{q}_{1,0}\Delta q_1) + b_{112}(t)(q_{1,0}\Delta\dot{q}_2 + \dot{q}_{2,0}\Delta q_1)\\
&\quad + b_{121}(t)(q_{2,0}\Delta\dot{q}_1 + \dot{q}_{1,0}\Delta q_2) + 3d_{1111}q_{1,0}^2\Delta q_1\\
&\quad + (d_{1112} + d_{1121} + d_{1211})(2q_{1,0}q_{2,0}\Delta q_1 + q_{1,0}^2\Delta q_2)\\
&\quad + g_{1111}(2\dot{q}_{1,0}q_{1,0}\Delta\dot{q}_1 + \dot{q}_{1,0}^2\Delta q_1 + 2\ddot{q}_{1,0}q_{1,0}\Delta q_1 + q_{1,0}^2\Delta\ddot{q}_1)\\
&\quad + g_{1211}(2\dot{q}_{1,0}q_{2,0}\Delta\dot{q}_1 + \dot{q}_{1,0}^2\Delta q_2 + \ddot{q}_{1,0}q_{2,0}\Delta q_1 + q_{1,0}\ddot{q}_{1,0}\Delta q_2 + q_{1,0}q_{2,0}\Delta\ddot{q}_1) = 0,
\end{aligned}
\tag{16}
$$

$$
\begin{aligned}
&M_2(\Delta\ddot{q}_2 + 2\zeta_2\omega_2\Delta\dot{q}_2 + \omega_2^2\Delta q_2) + c_{21}(t)\Delta\dot{q}_1 + k_{21}(t)\Delta q_1 + k_{22}(t)\Delta q_2\\
&\quad + 2a_{211}(t)q_{1,0}\Delta q_1 + (a_{212}(t) + a_{221}(t))(q_{1,0}\Delta q_2 + q_{2,0}\Delta q_1)\\
&\quad + b_{211}(t)(q_{1,0}\Delta\dot{q}_1 + \dot{q}_{1,0}\Delta q_1) + b_{212}(t)(q_{1,0}\Delta\dot{q}_2 + \dot{q}_{2,0}\Delta q_1)\\
&\quad + b_{221}(t)(q_{2,0}\Delta\dot{q}_1 + \dot{q}_{1,0}\Delta q_2) + 3d_{2111}q_{1,0}^2\Delta q_1\\
&\quad + (d_{2112} + d_{2121} + d_{2211})(2q_{1,0}q_{2,0}\Delta q_1 + q_{1,0}^2\Delta q_2)\\
&\quad + g_{2111}(2\dot{q}_{1,0}q_{1,0}\Delta\dot{q}_1 + \dot{q}_{1,0}^2\Delta q_1 + 2\ddot{q}_{1,0}q_{1,0}\Delta q_1 + q_{1,0}^2\Delta\ddot{q}_1)\\
&\quad + g_{2211}(2\dot{q}_{1,0}q_{2,0}\Delta\dot{q}_1 + \dot{q}_{1,0}^2\Delta q_2 + \ddot{q}_{1,0}q_{2,0}\Delta q_1 + q_{1,0}\ddot{q}_{1,0}\Delta q_2 + q_{1,0}q_{2,0}\Delta\ddot{q}_1) = 0.
\end{aligned}
\tag{17}
$$

The equations for the perturbation (16) and (17) may be recast into the following state vector formulation

$$\dot{\mathbf{v}}(t) = \mathbf{A}(t)\mathbf{v}(t),$$

$$
\mathbf{v}(t) = [\Delta q_1(t)\ \Delta q_2(t)\ \Delta\dot{q}_1(t)\ \Delta\dot{q}_2(t)]^{\mathrm{T}}, \quad \mathbf{A}(t) = \begin{bmatrix} \mathbf{I} & \mathbf{0} \\ \mathbf{0} & \mathbf{M}(t) \end{bmatrix}^{-1} \begin{bmatrix} \mathbf{0} & \mathbf{I} \\ -\mathbf{K}(t) & -\mathbf{C}(t) \end{bmatrix},
\tag{18}
$$

where the components of $\mathbf{K}(t)$, $\mathbf{C}(t)$ and $\mathbf{M}(t)$ are given as

$$
\begin{aligned}
K_{11}(t) &= M_1\omega_1^2 + k_{11} + 2a_{111}q_{1,0} + (a_{112} + a_{121})q_{2,0} + b_{111}\dot{q}_{1,0} + b_{112}\dot{q}_{2,0} + 3d_{1111}q_{1,0}^2\\
&\quad + 2(d_{1112} + d_{1121} + d_{1211})q_{1,0}q_{2,0} + g_{1111}(\dot{q}_{1,0}^2 + 2\ddot{q}_{1,0}q_{1,0}) + g_{1211}\ddot{q}_{1,0}q_{2,0},\\
K_{12}(t) &= k_{12} + (a_{112} + a_{121})q_{1,0} + b_{121}\dot{q}_{1,0}\\
&\quad + (d_{1112} + d_{1121} + d_{1211})q_{1,0}^2 + g_{1211}(\dot{q}_{1,0}^2 + q_{1,0}\ddot{q}_{1,0}),\\
K_{21}(t) &= k_{21} + 2a_{211}q_{1,0} + (a_{212} + a_{221})q_{2,0} + b_{211}\dot{q}_{1,0} + b_{212}\dot{q}_{2,0} + 3d_{2111}q_{1,0}^2\\
&\quad + 2(d_{2112} + d_{2121} + d_{2211})q_{1,0}q_{2,0} + g_{2111}(\dot{q}_{1,0}^2 + 2\ddot{q}_{1,0}q_{1,0}) + g_{2211}\ddot{q}_{1,0}q_{2,0},\\
K_{22}(t) &= M_2\omega_2^2 + k_{22} + (a_{212} + a_{221})q_{1,0} + b_{221}\dot{q}_{1,0}\\
&\quad + (d_{2112} + d_{2121} + d_{2211})q_{1,0}^2 + g_{2211}(\dot{q}_{1,0}^2 + q_{1,0}\ddot{q}_{1,0}),
\end{aligned}
\tag{19}
$$

$$
\begin{aligned}
C_{11}(t) &= 2M_1\zeta_1\omega_1 + b_{111}q_{1,0} + b_{121}q_{2,0} + 2g_{1111}\dot{q}_{1,0}q_{1,0} + 2g_{1211}\dot{q}_{1,0}q_{2,0},\\
C_{12}(t) &= c_{12} + b_{112}q_{1,0},\\
C_{21}(t) &= c_{21} + b_{211}q_{1,0} + b_{221}q_{2,0} + 2g_{2111}\dot{q}_{1,0}q_{1,0} + 2g_{2211}\dot{q}_{1,0}q_{2,0},\\
C_{22}(t) &= 2M_2\zeta_2\omega_2 + b_{212}q_{1,0},
\end{aligned}
\tag{20}
$$

$$
\begin{aligned}
M_{11}(t) &= M_1 + g_{1111}q_{1,0}^2 + g_{1211}q_{1,0}q_{2,0},\\
M_{12} &= 0,\\
M_{21}(t) &= g_{2111}q_{1,0}^2 + g_{2211}q_{1,0}q_{2,0},\\
M_{22} &= M_2.
\end{aligned} \tag{21}
$$

Solving Eq. (11) for $q_{1,0}(t)$ and $q_{2,0}(t)$, the time-dependent components of $\mathbf{K}(t)$, $\mathbf{C}(t)$ and $\mathbf{M}(t)$ are found, and the linearized equations (16) and (17) may be solved. The stability of the system may then be evaluated by the Floquet theory in case of periodic response [3] or by Lyapunov exponents as described by Wolf et al. [4].

Next, the numerical analyses are carried out with independent variation of the frequency ratios ω_0/ω_1, ω_2/ω_1 and with ω_0/Ω_0 and $u_0 = 0.3$ and 0.5 m. In light of the previous analysis showing the insufficiency of the Floquet theory, stability boundaries are in all cases found using Lyapunov exponents. In all the following analyses the circular eigenfrequency of the first mode is kept constant at $\omega_1 = 5.14\,\mathrm{rad/s}$. At the numerical integration, Eqs. (11) and (18) are solved simultaneously. The rms values of the response Q_1 and Q_2 are determined using time series of 1000 excitation periods T_0.

The first analysis is made with constant excitation ratio $\omega_0/\Omega_0 = 3.0$. The result is illustrated in Fig. 4 in terms of contour curves of the various response quantities. Figs. 4a and b show contour curves of Q_1 at 5, 10 and 20 m and Q_2 at 0.5, 2 and 4 m as functions of ω_0/ω_1 and ω_2/ω_1. In Fig. 4c the contour curve at 0 is shown for the largest Lyapunov exponent, indicating areas where the solution is unstable. The regions indicated by (▒) show where chaotic response occurs and (■) indicates regions with infinite response. Since ω_1 is kept constant and only ω_2 is varied in the fraction ω_2/ω_1, the positions of resonance peaks of the first mode are independent of ω_2/ω_1. Correspondingly, the positions of resonance peaks of the second mode vary linearly with ω_2/ω_1. In Fig. 4a peaks are present at $\omega_0/\omega_1 \simeq 0.75$ and 1.0, which remain constant to variations in ω_2/ω_1, and hence represent resonance peaks of the first mode. At frequencies $\omega_0/\omega_1 > 1.1$ large regions of unstable response occur. The limit $\omega_0/\omega_1 = 1.1$ is relatively constant with variation of ω_2/ω_1. Within the region $\omega_0/\omega_1 > 1.1$ two different areas exist divided by an almost constant line with respect to variation of ω_0/ω_1 located at $\omega_2/\omega_1 \simeq 2.2$. Below this limit the system produces infinite response in most part of the unstable region, while above the limit chaotic response exists in all unstable regions. Close to the boundary at $\omega_2/\omega_1 \simeq 2.2$ large regions of stable response exist even above $\omega_0/\omega_1 > 1.1$.

Figs. 5a–c show contour curves for Q_1, Q_2 and λ with $u_0 = 0.3$ m, a constant eigenfrequency ratio $\omega_2/\omega_1 = 2.0$, and with variable excitation ratio ω_0/Ω_0. Looking at the figures from left to right it is seen that the primary resonance peaks located at $\omega_0/\omega_1 = 0.75$ and 1.0 are relatively unaffected by the excitation ratio. The combined peak at $\omega_0/\omega_1 = 1.5$ tends to divide into two peaks as ω_0/Ω_0 are varied from 3.0. Finally, the large unstable region to the far right is stabilized as the excitation ratio is increased, while the unstable region at $\omega_0/\omega_1 \simeq 1.25$ stabilizes with increasing ω_0/Ω_0. It should be noted that all unstable regions produce chaotic response with $\omega_2/\omega_1 = 2.0$, except for a large region at the bottom right, which produces infinite response. No instability occurs below $\omega_0/\omega_1 = 1.1$, except for a small region at $\omega_0/\omega_1 \simeq 0.9$ and $\omega_0/\Omega_0 \simeq 2.5$.

Figs. 6a–c show Q_1, Q_2 and λ, respectively with $\omega_2/\omega_1 = 2.2$. Comparing with the results of Fig. 5 it is seen that all unstable regions produce chaotic response. Also, the amplitude of the response is significantly reduced, especially $Q_2 < 2$ m in the considered parameter space. Also in this case the main regions at $\omega_0/\omega_1 > 1.1$ are unstable. However, regions around $\omega_0/\omega_1 = 1.5$ and 2.1 produce stable response. Within these stable regions relatively large response is produced compared with the surrounding chaotic regions.

Finally, the corresponding analysis as shown in Figs. 5 and 6 are carried out with $u_0 = 0.5$ m. Stability regions defined by λ are shown in Figs. 7a and b with $\omega_2/\omega_1 = 2.0$ and $\omega_2/\omega_1 = 2.2$, respectively. Comparing Fig. 7a with Fig. 5c reveals that, no significant changes are seen on the stability regions at $\omega_0/\omega_1 < 1.5$. The regions with infinite response is slightly increased due to the influence of quadratic parametric terms.

Comparing Fig. 7b with Fig. 6c shows that for $\omega_2/\omega_1 = 2.2$ no significant changes of the stability regions occur while increasing u_0. It should be noted that no regions with infinite response occur.

To validate the stability determined by Lyapunov exponents, stability is determined as function of u_0 and ζ_1 with $\omega_0/\Omega_0 = 3.0$, $\omega_2/\omega_1 = 2.2$ and $\omega_0/\omega_1 = 1.7$. While simulating the response the periodicity of the

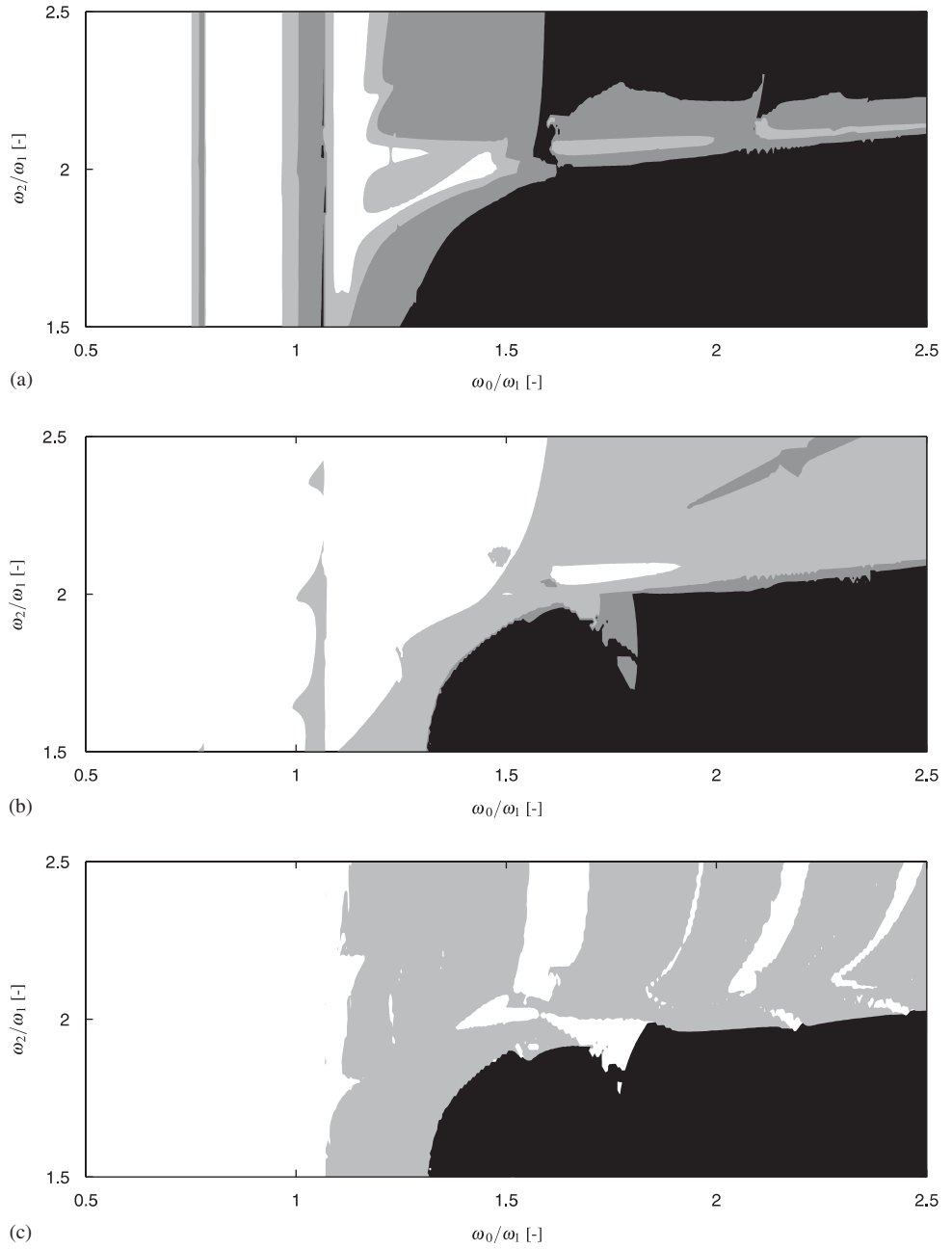

Fig. 4. Contour curves for analysis made with constant excitation ratio $\omega_0/\Omega_0 = 3.0$. $u_0 = 0.3$ m. (a) Q_1 [m]. (▒) $Q_1 > 5$ m, (▒)$Q_1 > 10$ m, (■) $Q_1 > 20$ m. (b) Q_2 [m]. (▒) $Q_2 > 0.5$ m, (▒) $Q_2 > 2$ m, (■) $Q_2 > 4$ m. (c) Largest Lyapunov exponent λ [-]. (■) $\lambda > 0$, (■) infinite response.

response is investigated by a residual r given as

$$r = ((q_1(t) - q_1(t+T))^2 + (q_2(t) - q_2(t+T))^2 + (\dot{q}_1(t) - \dot{q}_1(t+T))^2 + (\dot{q}_2(t) - \dot{q}_2(t+T))^2)^{1/2}, \quad (22)$$

where T is found from Eq. (14). The residual r is an indication of the periodicity of the response assuming that T is the response period, i.e. if $r = 0$ the response is periodic. Since the analysis is made by means of numerical

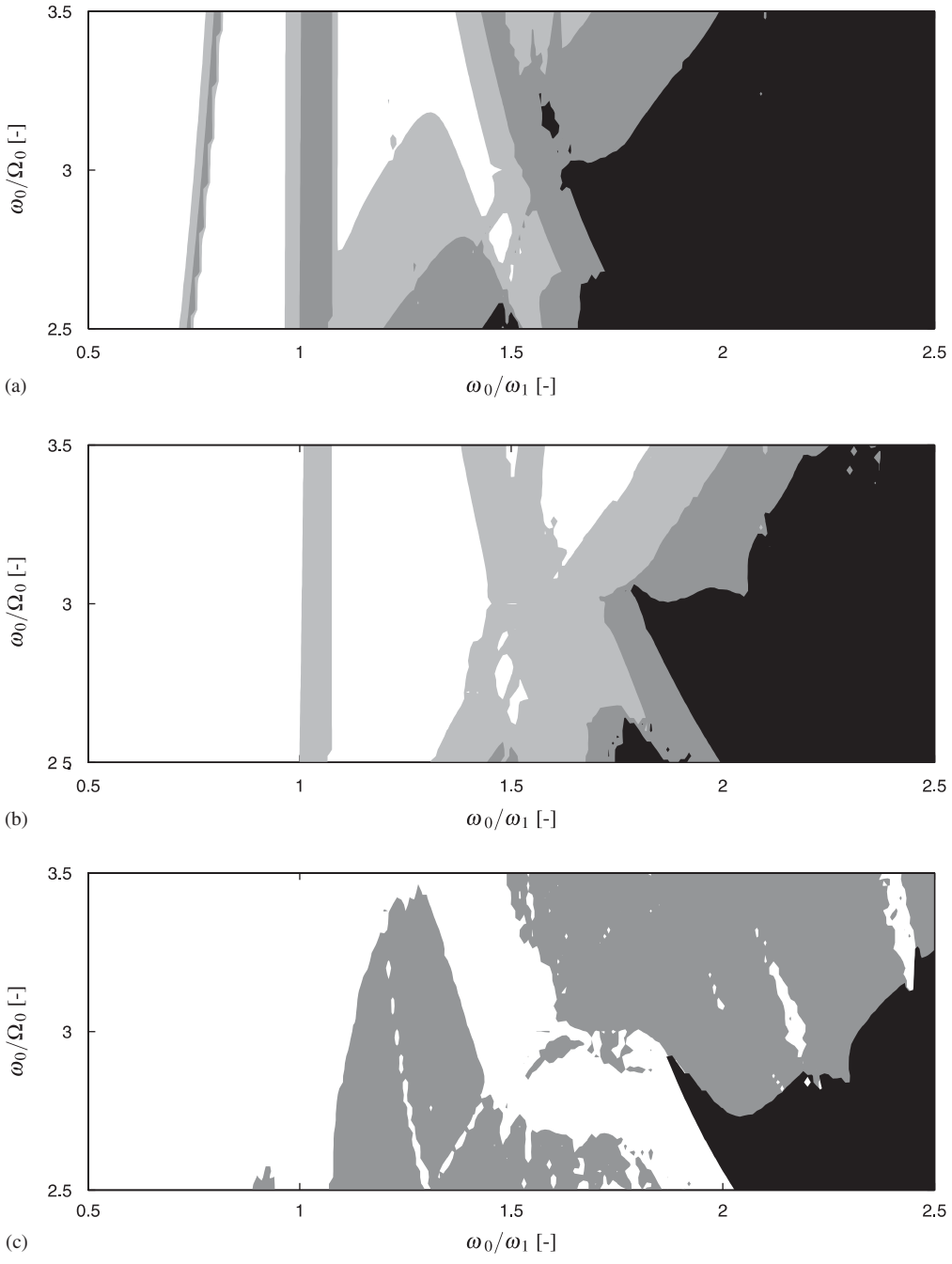

Fig. 5. Contour curves for analysis made with constant eigenfrequency ratio $\omega_2/\omega_1 = 2.0$. $u_0 = 0.3$ m. (a) Q_1 [m]. (▒) $Q_1 > 5$ m, (▒) $Q_1 > 10$ m, (■) $Q_1 > 20$ m. (b) Q_2 [m]. (▒) $Q_2 > 0.5$ m, (▒) $Q_2 > 2$ m, (■) $Q_2 > 4$ m. (c) Largest Lyapunov exponent λ [-]. (▒) $\lambda > 0$, (■) infinite response.

integration, an upper limit of r is defined for the response to be assumed periodic with the period T. A periodic response is assumed when $r < 0.001$. When $r > 0.001$ non-periodic response is assumed. The result is shown in Fig. 8 where (▒) indicates regions with $\lambda > 0$ and (—) is the contour line for $r = 0.001$. The residual assumes that the period T is determined from Eq. (14), this might not be the case while including nonlinear terms. However, the numerical simulations show good agreement between the stability boundary determined by the residual and determined by the Lyapunov exponent.

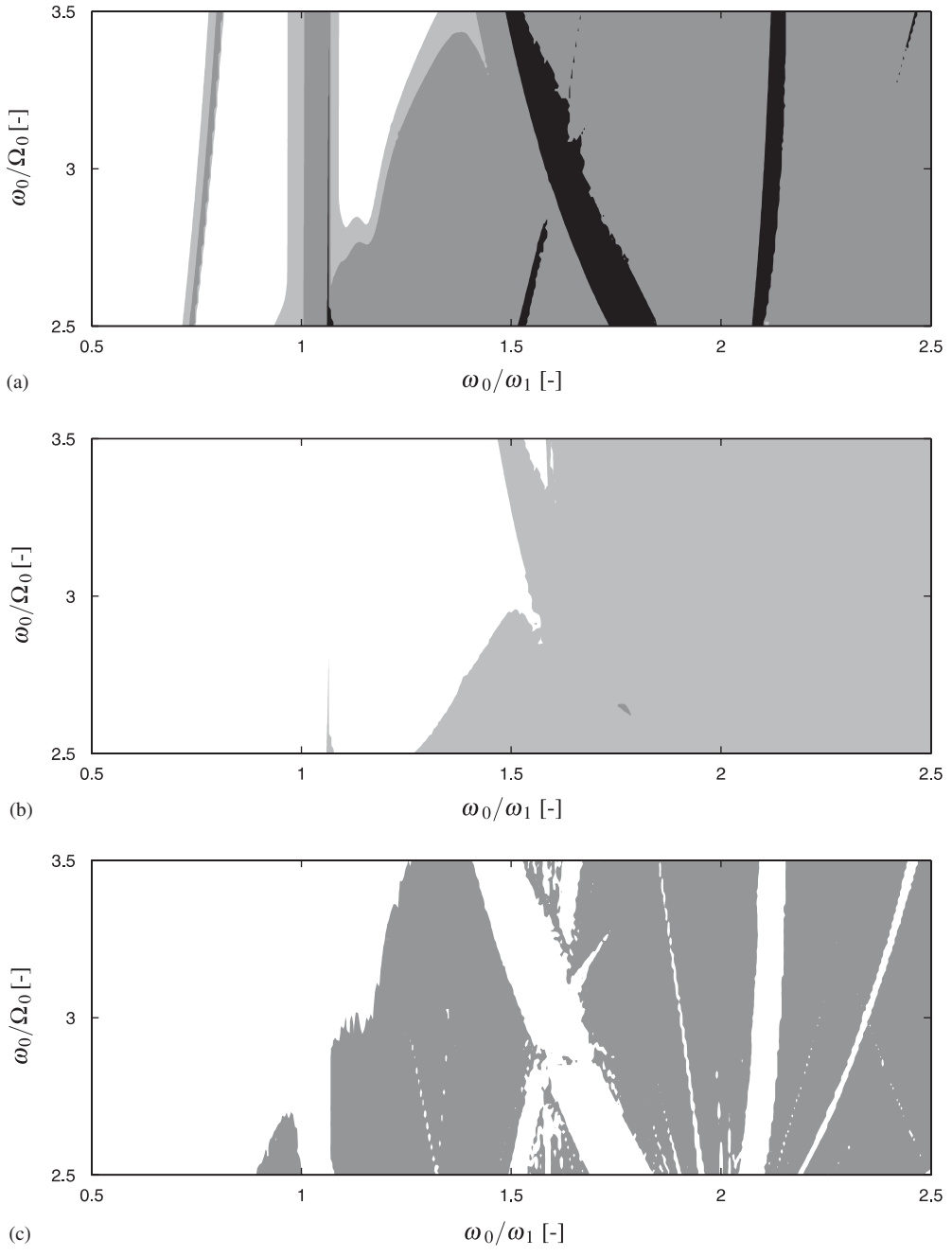

Fig. 6. Contour curves for analysis made with constant eigenfrequency ratio $\omega_2/\omega_1 = 2.2$. $u_0 = 0.3$ m. (a) Q_1 [m]. (▒) $Q_1 > 5$ m, (▒) $Q_1 > 10$ m, (■) $Q_1 > 20$ m. (b) Q_2 [m]. (▒) $Q_2 > 0.5$ m, (▒) $Q_2 > 2$ m, (■) $Q_2 > 4$ m. (c) Largest Lyapunov exponent λ [-]. (▒) $\lambda > 0$, (■) infinite response.

5. Concluding remarks

The nonlinear parametric instability of a wind turbine wing model as a 2dof system retaining up to cubic terms has been analysed at various excitation ratios between the support point excitation frequency and the rotational frequency of the rotor and at various eigenfrequency ratios.

For ordinary three-bladed wind turbines, the dominating tower frequency in proportion to the rotational frequency is close to 3. For large wind turbines the eigenfrequency ratio of the fundamental modes may be

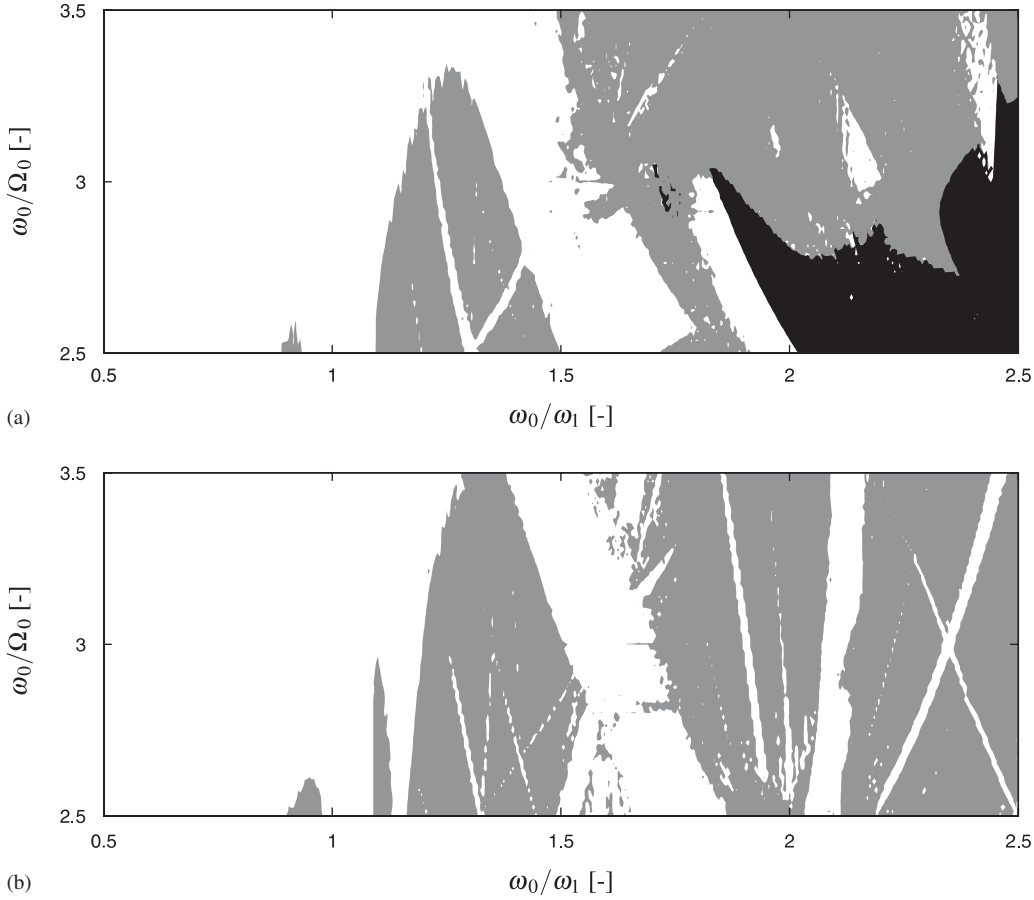

Fig. 7. Contour curves for $\lambda = 0$ at various constant eigenfrequency ratio. $u_0 = 0.5$ m. (■) $\lambda > 0$, (■) infinite response. (a) $\omega_2/\omega_1 = 2.0$, (b) $\omega_2/\omega_1 = 2.2$.

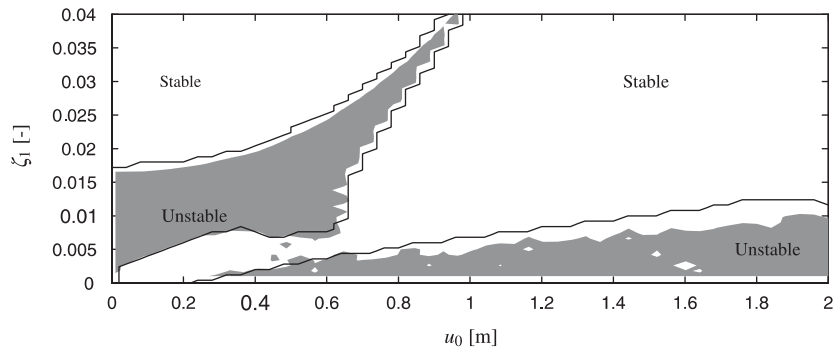

Fig. 8. Contour curves for λ and r. $\omega_2/\omega_1 = 2.2$, $\omega_0/\Omega_0 = 3.0$, $\omega_0/\omega_1 = 1.7$. (■) $\lambda > 0$, (—) contour line for $r = 0.001$.

close to 2. Since this may introduce 2:1 internal resonance, the numerical analysis is centred around these frequency ratios.

It is shown that the parametric instability mainly is influenced by quadratic parametric terms. These terms may produce large regions of chaotic response for fixed excitation ratios. Furthermore, it is shown that cubic nonlinear terms have a significant stabilizing effect at given resonance frequencies.

At irrational excitation ratios the response is shown to be almost periodic. Hence, the Floquet theory is not applicable for analysing the stability of the system. At rational excitation ratios the response becomes periodic. However, the Floquet theory is only useful for finding stability boundaries in case of relatively short response periods. Instead, the theory of Lyapunov exponents is used for analysing the stability of the system.

Using numerical simulations it is shown that within a relatively small frequency band around $\omega_2/\omega_1 = 2.2$ stable regions appear for $\omega_0/\omega_1 > 1.1$ in all other cases unstable response mainly occur in this region. With $\omega_2/\omega_1 > 2.2$ chaotic response is produced while the response becomes infinite at $\omega_2/\omega_1 < 2.2$. No significant changes of the stability regions appear when increasing u_0 except for smaller regions, which change character from chaotic to infinite response when $\omega_2/\omega_1 = 2.0$.

The indicated results refer to a 2dof reduced system including only the two lowest fundamental modes. The reduced model is convenient when working with control algorithms of wind turbines where only a few modes are observable. However, at resonance excitation frequencies, energy may transfer to higher modes via nonlinear couplings. The energy leakage from lower to higher modes may introduce qualitative and quantitative changes to the frequency response. The effect of this energy leakage on the qualitative and quantitative results presented in the study will be further analysed in a succeeding study.

Acknowledgements

This work has been supported by the Danish Technical Research Council through the project Damping Mechanisms in Dynamics of Structures and Materials.

Appendix A. Wing specifications

The theory is demonstrated using a 46 m wing. The aerodynamic profiles are NACA 63-418 section profile as illustrated in Fig. 11, scaled with chord and height values indicated in Fig. 12d. The inner 2.0 m of the wing has a circular cross section with 2.0 m in diameter. The wing has a total weight of 10 t. The stiffness and mass distribution are chosen so that the eigenfrequencies match approximately to those given by the manufacture of a corresponding wing size. The twist throughout the wing is chosen so that the angle of attack of the resulting wind is approximately 6° at a constant rotational speed of $1.6\,\mathrm{s}^{-1}$, and an incoming wind velocity of 12 m/s. The elasticity module is constant throughout the wing given as $E = 3 \times 10^{10}$ Pa (Figs. 9–12).

The fundamental blade and edgewise eigenmodes are illustrated in Fig. 9. The components in the x_1' and x_2' directions are shown in Fig. 10 with the dominating components normalized to 1 at the wing tip. The components determined by the Bernoulli–Euler beam theory are plotted as (——) and (—) for the component in the x_1' and x_2' directions, respectively. As seen, a considerable edgewise component is present in the blade mode $\Phi^{(1)}$ and an even more dominating blade component is present in the edgewise mode $\Phi^{(2)}$. The circular eigenfrequency of the first mode is 5.14 rad/s and the modal masses are $M_1 = 427.9$ and $M_2 = 852.1$ kg. The wing has the twist angle, the mass, local moments of inertia, chord length and thickness distributions as indicated in Fig. 12. The structural damping in the edgewise mode is kept constant at the modal damping ratio $\zeta_2 = 0.01$. The lift and drag coefficients are assumed to be

$$c_L = 1.5, \quad c_D = 0.05. \tag{A.1}$$

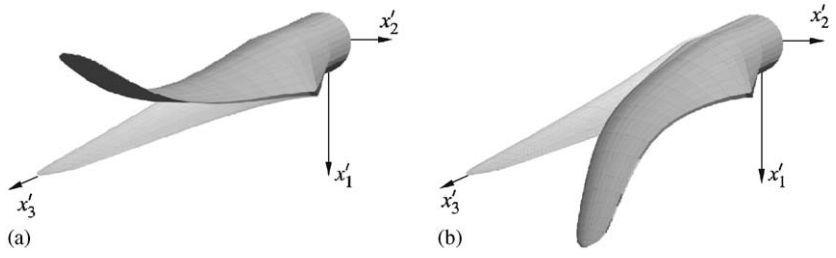

Fig. 9. (a) First eigenmode $\Phi^{(1)}$, (b) second eigenmode $\Phi^{(2)}$.

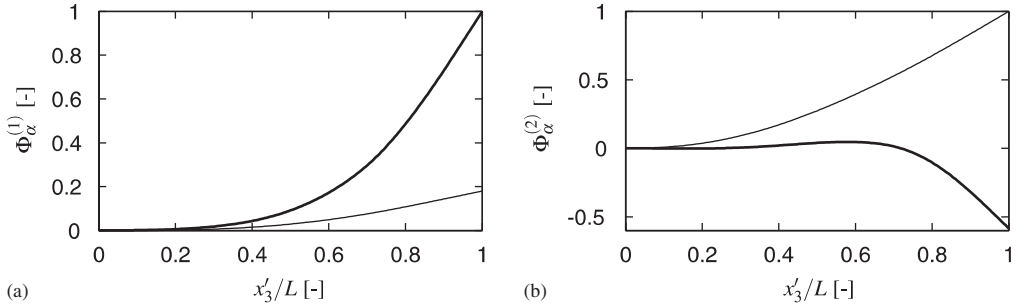

Fig. 10. Components of eigenmodes. (——) Φ_1, (—) Φ_2. (a) First eigenmode $\Phi^{(1)}$, (b) second eigenmode $\Phi^{(2)}$.

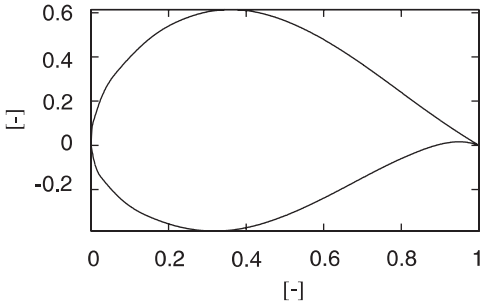

Fig. 11. Normalized profile of a NACA 63-418 wing section.

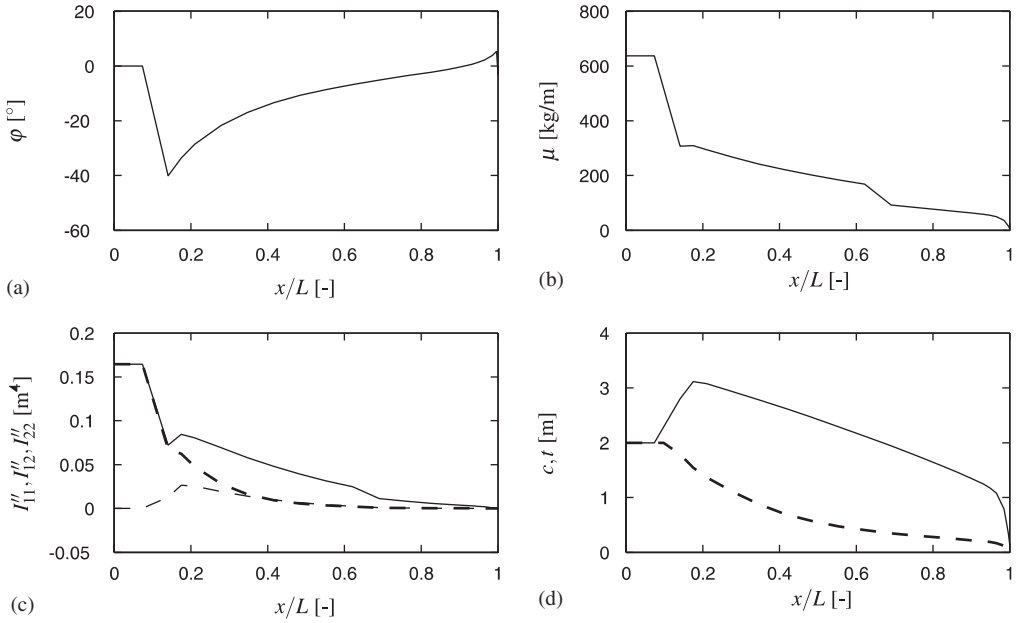

Fig. 12. (a) Twist angle throughout the beam, (b) mass per unit length, (c) distribution of local moment of inertia. (—) I_{11}'', (– –) I_{12}'', (— —) I_{22}''. (d) (—) Chord length c. (— —) Thickness t of cross-sections.

Appendix B. Time-dependent coefficients

Harmonic support point motion given in Eq. (12) is assumed in addition to harmonic variation of the aerodynamic loading then, the time varying coefficients $c_{ij}(t)$, $k_{ij}(t)$, $a_{ijk}(t)$, $b_{ijk}(t)$ and $f_i(t)$ given in Eqs. (8)

and (10) may be written as

$$\begin{aligned}
k_{ij}(t) = & -k_{ij,11}\Theta_{2,0}^2\dot{u}^2(t) + k_{ij,12}\Theta_{2,0}(\ddot{u}(t)\sin\Omega_0 t + \dot{u}(t)\Omega_0\cos\Omega_0 t) \\
& + k_{ij,21}\Theta_{2,0}(-\ddot{u}(t)\sin\Omega_0 t + \dot{u}(t)\Omega_0\cos\Omega_0 t) \\
& + k_{ij,22}(-\Theta_{2,0}^2\dot{u}^2(t)\sin^2\Omega_0 t - \Omega_0^2) + k_{ij,33}\Theta_{2,0}^2\dot{u}^2(t)\cos^2\Omega_0 t, \\
c_{ij}(t) = & -c_{ij,1}\dot{u}(t)\Theta_{2,0}\sin\Omega_0 t, \\
a_{ijk}(t) = & a_{ijk,0}(t) - a_{ijk,1}\Theta_{2,0}(\ddot{u}(t)\cos\Omega_0 t + \dot{u}(t)\Omega_0\sin\Omega_0 t) - a_{ijk,2}\Theta_{2,0}^2\dot{u}^2(t)\sin\Omega_0 t\cos\Omega_0 t, \\
b_{ijk}(t) = & -b_{ijk,1}\Theta_{2,0}\dot{u}(t)\cos\Omega_0 t + b_{ijk,2}\Omega_0, \\
f_i(t) = & f_{i,0}(t) + f_{i,1}\Theta_{2,0}(\ddot{u}(t)\cos\Omega_0 t - \Omega_0\dot{u}(t)\sin\Omega_0 t) - f_{i,2}\Theta_{2,0}^2\dot{u}^2(t)\sin\Omega_0 t\cos\Omega_0 t + f_{i,3}\ddot{u}(t),
\end{aligned} \tag{B.1}$$

where the time-independent coefficients are found to be

$$\begin{aligned}
c_{ij,1} &= 2\int_0^L \mu(-\Phi_1^{(i)}\Phi_2^{(j)} + \Phi_2^{(i)}\Phi_1^{(j)})\,\mathrm{d}x_3', \\
k_{ij,\alpha\beta} &= \int_0^L \mu\Phi_\alpha^{(i)}\Phi_\beta^{(j)}\,\mathrm{d}x_3', \quad k_{ij,33} = \int_0^L \left[\frac{\partial\Phi_\alpha^{(i)}}{\partial x_3'}\frac{\partial\Phi_\alpha^{(j)}}{\partial x_3'}\int_{x_3'}^L \mu x_3'\,\mathrm{d}x_3'\right]\mathrm{d}x_3', \\
a_{ijk,\alpha} &= \int_0^L \left[\frac{\partial\Phi_\beta^{(i)}}{\partial x_3'}\frac{\partial\Phi_\beta^{(j)}}{\partial x_3'}\int_{x_3'}^L -\mu\Phi_\alpha^{(k)}\,\mathrm{d}x_3'\right]\mathrm{d}x_3', \quad b_{ijk,\alpha} = 2a_{ijk,\alpha}, \\
f_{i,\alpha} &= -\int_0^L \Phi_\alpha^{(i)}\mu x_3'\,\mathrm{d}x_3', \quad f_{i,3} = \int_0^L \Phi_1^{(i)}\mu\,\mathrm{d}x_3'.
\end{aligned} \tag{B.2}$$

The incoming wind velocity $V_1'(x_3', t)$ as seen from a considered cross section of the wing varies periodically with the rotational speed Ω_0. $V_1'(x_3', t)$ is assumed to vary logarithmically in the following way

$$V_1'(x_3', t) = V_0\frac{\ln x_3}{\ln h} = V_0\frac{\ln(h - x_3'\cos\Omega_0 t)}{\ln h}, \tag{B.3}$$

where V_0 is the undisturbed mean wind velocity and h is the height of the rotor axis. The rotational wind velocity is given as $V_2'(x_3') = x_3'\Omega_0$. Then, the resulting wind velocity $V(x_3', t)$ may be written as

$$V(x_3', t) = \sqrt{V_1'^2(x_3', t) + V_2'^2(x_3')}. \tag{B.4}$$

Based on Eq. (B.4) the following expression for the aerodynamic loads is derived:

$$p_{1,A}''(x_3', t) = \frac{1}{2}\rho V^2(x_3', t)c(x_3')c_L \simeq p_{1,A,0}''(x_3') + \Delta p_{1,A,1}''(x_3')\cos\Omega_0 t,$$

$$p_{2,A}''(x_3', t) = \frac{1}{2}\rho V^2(x_3', t)c(x_3')c_D \simeq p_{2,A,0}''(x_3') + \Delta p_{2,A,1}''(x_3')\cos\Omega_0 t. \tag{B.5}$$

$p_{\alpha,A,0}''(x_3')$ denotes the mean value of $p_{\alpha,A}''(x_3', t)$, when the wing is at the top and bottom positions. Correspondingly, $\Delta p_{\alpha,A,1}''(x_3')$ denotes half of the difference between these extreme values. c_L and c_D are the lift and drag coefficients. The coefficients $a_{ijk,0}(t)$ and $f_{i,0}(t)$ in Eq. (B.1) may then be written in the following way:

$$a_{ijk,0}(t) = a_{ijk,00} + \Delta a_{ijk,01}\cos\Omega_0 t, \quad f_{i,0}(t) = f_{i,00} + \Delta f_{i,01}\cos\Omega_0 t \tag{B.6}$$

with

$$a_{ijk,00} = \int_0^L \left[\frac{\partial \Phi_\alpha^{(i)}}{\partial x_3'} \frac{\partial \Phi_\alpha^{(j)}}{\partial x_3'} \int_{x_3'}^L \left[-p''_{\beta,A,0} \frac{\partial \Phi_\beta^{(k)}}{\partial x_3'} \right] \mathrm{d}x_3' + \frac{1}{2} \Phi_\alpha^{(i)} p''_{\beta,A,0} \frac{\partial \Phi_\alpha^{(j)}}{\partial x_3'} \frac{\partial \Phi_\beta^{(k)}}{\partial x_3'} \right] \mathrm{d}x_3',$$

$$\Delta a_{ijk,01} = \int_0^L \left[\frac{\partial \Phi_\alpha^{(i)}}{\partial x_3'} \frac{\partial \Phi_\alpha^{(j)}}{\partial x_3'} \int_{x_3'}^L \left[-\Delta p''_{\beta,A,1} \frac{\partial \Phi_\beta^{(k)}}{\partial x_3'} \right] \mathrm{d}x_3' + \frac{1}{2} \Phi_\alpha^{(i)} \Delta p''_{\beta,A,1} \frac{\partial \Phi_\alpha^{(j)}}{\partial x_3'} \frac{\partial \Phi_\beta^{(k)}}{\partial x_3'} \right] \mathrm{d}x_3',$$

$$f_{i,00} = \int_0^L \Phi_\alpha^{(i)} p''_{\alpha,A,0} \, \mathrm{d}x_3', \quad \Delta f_{i,01} = \int_0^L \Phi_\alpha^{(i)} \Delta p''_{\alpha,A,1} \, \mathrm{d}x_3'. \tag{B.7}$$

References

[1] J.W. Larsen, S.R.K. Nielsen, Nonlinear dynamics of wind turbine wings, *International Journal of Non-Linear Mechanics* 41(5) (2006) 629–634.

[2] A.H. Nayfeh, *Nonlinear Interactions, Analytical, Computational, and Experimental Methods*, Wiley, New York, 2000.

[3] A.H. Nayfeh, D.T. Mook, *Nonlinear Oscillations*, Wiley, New York, 1995.

[4] A. Wolf, J.B. Swift, H.L. Swinney, J.A. Vastano, Determining Lyapunov exponents from a time series, *Physica D* 16 (1985) 285–317.

[5] F.C. Moon, *Chaotic Vibrations. An Introduction for Applied Scientists and Engineers*, Wiley, New York, 1987.

[6] J.J. Thomsen, *Vibrations and Stability*, McGraw-Hill, New York, 1997.

[7] C.W.S. To, M.L. Liu, Lyapunov exponents and information dimensions of multi-degree-of-freedom systems under deterministic and stationary random excitations, *IUTAM Symposium on Advances in Nonlinear Stochastic Mechanics*, 1996 pp. 449–458.

[8] M. Castanier, C. Pierre, Lyapunov exponents and localization phenomena in multi-coupled nearly periodic systems, *Journal of Sound and Vibration* 183 (3) (1995) 493–515.

[9] K. Shin, J.K. Hammond, The instantaneous Lyapunov exponent and its application to chaotic dynamical systems, *Journal of Sound and Vibration* 218 (3) (1998) 389–403.

[10] Z.M. Ge, P.C. Tsen, Non-linear dynamic analysis and control of chaos for a two-degrees-of-freedom rigid body with vibrating support, *Journal of Sound and Vibration* 240 (2) (2001) 323–349.

[11] Z.M. Ge, J.S. Shiue, Non-linear dynamic and control of chaos for a tachometer, *Journal of Sound and Vibration* 253 (4) (2002) 773–793.

[12] S. Dwivedy, R. Kar, Dynamics of a slender beam with an attached mass under combination parametric and internal resonances—part I: steady state response, *Journal of Sound and Vibration* 221 (5) (1999) 823–848.

[13] S. Dwivedy, R. Kar, Dynamics of a slender beam with an attached mass under combination parametric and internal resonances part—II: periodic and chaotic response, *Journal of Sound and Vibration* 222 (2) (1999) 281–305.

[14] S.K. Dwivedy, R.C. Kar, Nonlinear response of a parametrically excited system using higher-order method of multiple scales, *Nonlinear Dynamics* 20 (1999) 115–130.

[15] S.K. Dwivedy, R.C. Kar, Simultaneous combination, principal parametric and internal resonances in a slender beam with a lumped mass: three-mode interactions, *Journal of Sound and Vibration* 242 (1) (2001) 27–46.

[16] S.K. Dwivedy, R.C. Kar, Nonlinear dynamics of a cantilever beam carrying an attached mass with 1:3:9 internal resonance, *Nonlinear Dynamics* 31 (2003) 49–72.

[17] A.H. Nayfeh, The response of multidegree-of-freedom systems with quadratic non-linearities to a parametric excitation, *Journal of Sound and Vibration* 88 (1983) 547–557.

[18] A.H. Nayfeh, The response of multidegree-of-freedom systems with quadratic non-linearities to a harmonic parametric resonance, *Journal of Sound and Vibration* 90 (1983) 237–244.

[19] S. Hanagud, S. Sarkar, Problem of the dynamics of a cantilever beam attached to a moving base, *Journal of Guidance, Control, and Dynamics* 13 (3) (1989) 438–441.